Special Issue: Research Article

advanced technologies

Received: 29 June 2010, Revised: 6 September 2010, Accepted: 6 September 2010, Published online in Wiley Online Library: 10 November 2010

(wileyonlinelibrary.com) DOI: 10.1002/pat.1849

Thermal decomposition study of poly(methyl methacrylate)/carbon nanofiller composites

A.O. Pozdnyakov[a,b]*, U.A. Handge[c], A. Konchits[d] and V. Altstädt[c]

This work compares the thermal degradation kinetics of neat atactic poly(methyl methacrylate) (a-PMMA), and its composites with fullerene C_{60} and multiwall carbon nanotubes (MWNT) as revealed by thermal desorption mass-spectrometry (TDMS), and thermal gravimetry analysis (TGA). TDMS suggests the decrease of thermal stability of PMMA-C_{60} composite compared to neat PMMA. This result is supported by the increased rate of defect formation in the composite as revealed by the electronic paramagnetic resonance, EPR, technique. On the other hand, TGA shows an increase of thermal degradation temperatures for composite compared to those of neat a-PMMA. The discrepancies between TDMS and TGA data are discussed taking into account the difference of the experimental conditions of the two approaches, i.e. the size of the sample. The parameters which need to be thoroughly controlled in thermal degradation kinetic studies are outlined. Copyright © 2010 John Wiley & Sons, Ltd.

Keywords: electron paramagnetic resonance; fullerene; mass-spectrometry; nanotube; polymer; thermal stability

INTRODUCTION

Fullerenes and other nanocarbon species are important in many areas of research.[1–3] In the case of sufficient dispersion, the use of these nanosized objects as fillers is expected to give new properties to the polymer matrices. Poly(methyl methacrylate)-fullerene and other poly(methyl methacrylate)-nanocarbon composites are attractive due to their possible applications in many fields, e.g. electronics and optoelectronics.[4] Introduction of C_{60} into PMMA is found to result in interesting phenomena, e.g. increase in PMMA glass transition temperature.[5] Stereoregularity plays an important role in the structural behavior of PMMA gels.[6] In the studies of PMMA-fullerene C_{60} composites it is also found that the stereoregularity and molecular weight of PMMA matrix influence the composite structure formation resulting, e.g. in peculiar PMMA-C_{60} peapod structures.[7] This opens the way to enhance the capacity of polymer matrices to store fullerene molecules. According to Reference [8] the thermodynamical approach of Flory[9] predicts the maximum volume fraction of molecularly dispersed fullerene C_{60} to be on the order of ~10% inside the polymer matrix.

Thermal degradation of PMMA is also related to stereoregularity and molecular weight of macromolecules.[10] In addition to filler dispersion state in the matrix, the thermal degradation of PMMA-C_{60} composite is therefore expected to be related to the structural peculiarities of macromolecules. Many works deal with these interesting questions.[11–17] However, the results of different studies are not consistent, e.g. due to the different experimental methods used to probe thermal stability, and need to be studied in more detail. Our work presents the comparison of the results of thermal decomposition study of PMMA and PMMA-C_{60} composites by means of thermal desorption mass-spectrometry (TDMS) and thermal gravimetry analysis (TGA) and discusses the discrepancies between the results of these methods.

EXPERIMENTAL

Fullerene C_{60} of 98% purity (Fullerene Technology Co., St. Petersburg) and CVD grown Arkema™ MWNT of purity > 90% were used as fillers. The matrix material was atactic commercial PMMA. The average molecular weight of the polymer was determined by means of gel permeation chromatography (Waters 510 pump, Waters Corp., Milford, MA, USA) with tetrahydrofuran (THF) as solvent to be M_n ~$8.8\,10^5$ g/mol with $M_w/M_n = 1.4$. The tacticities of a-PMMA (dissolved in deuterated chloroform) were determined by means of ^{1}H NMR spectrometry (Bruker Avance 300 spectrometer at 300.1 MHz) to be 5% iso, 40% hetero, and 55% syndio triads. The glass transition temperature ($T_g = 122^\circ$C) was measured by means of differential scanning calorimetry, DSC, at the second heating scan after solvent removal. T_g changes due to C_{60} incorporation in the matrix have not been registered.

* *Correspondence to: A. Pozdnyakov, Ioffe Physico-Technical Institute, 194021, Polytechnical str. 26, S-Petersburg, Russia.*
E-mail: ao.pozd@mail.ioffe.ru

a *A. Pozdnyakov*
Institute of the Problems of Mechanical Engineering, 199178, Bol'shoi pr. V.O., 61, S-Petersburg, Russia

b *A. Pozdnyakov*
Ioffe Physico-Technical Institute, 194021, Polytechnical str. 26, S-Petersburg, Russia

c *U. Handge, V. Altstädt*
Department of Polymer Engineering, Faculty of Engineering Science, University of Bayreuth, Universitätsstrasse 30, 95447 Bayreuth, Germany

d *A. Konchits*
Lashkarev Institute of Semiconductor Physics, NAS of Ukraine, Pr. Nauky 45, 03028, Kyiv, Ukraine

polymers advanced technologies

Reagent grade toluene was used to prepare the a-PMMA-nanofiller composite solutions. The solutions of neat components in toluene were prepared first. These solutions were co-dissolved and stirred in an ultrasonic cleaner VWR Int. at 45 Hz for 30 min. No visible sedimentation was observed during 1-2 weeks for composite solutions stored in a closed vessel. The solutions were cast on the surface of the degreased glass substrates to produce (after drying) films of ~5–100 μm thickness. Thicker films resulted from the pouring larger amounts of solution on the substrate and took longer time for solvent evaporation to form a film. We will refer to this regime as slow drying (SD) conditions. Thinner films were obtained by pouring lesser amounts of the solution and drying took less time. The latter conditions will be referred to as rapid drying (RD) conditions. After film formation they were additionally dried for ~5 hr at 80°C at a pressure of 400 mbar in a vacuum oven (Kendro Lab. Products). These films varied in color from pale violet (characteristic of RD composite films) to dark violet (SD composite films). The neat a-PMMA and PMMA-MWNT composite films we discuss below had intermediate thickness, i.e. were prepared in the regime intermediate to SD and RD conditions. The rated volume concentration of the fillers in the a-PMMA matrices was ~5–7%.

Transmission electron microscopy (TEM) investigations were carried out using a LEO EM 922 Omega (Carl Zeiss, Oberkochen, Germany) with an acceleration voltage of 200 kV. The thin films of the composites were embedded in an epoxy resin in order to prepare ultrathin cuts of the samples.

TDMS spectra were registered with time-of-flight MS of reflectron type with electron ionization, MSCh-6. The resolution ability of the spectrometer is about 800, electron ionization energy 70 eV. The principles of our TDMS experiment are described elsewhere.[12] As a substrate we used stainless steel foil (thickness ~100 μm, area ~0.5 × 0.5 cm^2) coated with the polymer coating (thickness, L, below ~1 μm) by light contact of the material with the surface of the foil. The calculations of average thickness are done from the dependence of MMA peak intensity on time (with account on the MMA ionization cross section) and the area of the surface covered with the film. This is possible since PMMA completely depolymerizes upon heating and the area under the MMA peak intensity is thus a direct measure of the quantity of the polymer subjected to heating. The substrate is resistively heated under given voltage-time program. In the experiments discussed below the heating regime was the same for all samples. The heating regime was the monotonous increase of the sample temperature at the rate of ~8 K s^{-1} at the maximum of the desorption rate. The temperature of the sample is measured by chromel-alumel thermocouple welded to the bottom side of the metal foil.

The rate of mass loss of the samples was registered by TGA/SDTA 851e (Mettler Toledo, Gießen, Germany) apparatus in a nitrogen atmosphere. The weight of the sample was approx. 10 mg. The tests were performed in the temperature range from 25–1100 °C with a heating rate of 10 K min^{-1}. Thermal transitions in the materials were registered with DSC Q1000 apparatus (TA Instruments, Eschborn, Germany) at a heating/cooling rate of 10 K/min. The measurements were performed in a nitrogen atmosphere. The temperature interval was 0–260 °C and a heating-cooling-heating cycle was applied. The net weight of the samples was in the order of 10 mg.

EPR measurements were carried out at room temperatures using X-band (microwave frequency $\nu \cong 9.4$GHz) EPR spectrometer Radiopan X-2244 with 100 kHz modulation of magnetic field. Estimated accuracy in the determination of the g-factor was $\pm 3\,10^{-4}$ for the observed EPR lines (line width $\Delta H_{pp} \leq 10$ G). The absolute accuracy of the spin density (N_s) was ±50%, whereas the relative accuracy of N_s at thermal destruction process of the specific sample was ± 20%. The heating of the samples was carried out in dynamic vacuum conditions at pressure of ~4 mbar.

Fourier transform infra red (FT-IR) spectra were recorded using a Nicolet Nexus 470 apparatus. The wave number range was 400–5000 cm^{-1} with a resolution of 1 cm^{-1}. X-ray diffraction measurements were carried out in the reflection mode in order to analyze the microstructure of neat PMMA and of the composites. X-ray diffractometer (PANalytical X-pert MPD Pro) equipped with CuK_α radiation source ($\lambda = 0.15418$ nm) was used (operation parameters 40 kV and 40 mA). The measurements were performed in the interval $2\theta = 5–55°$ with an increment of 0.008°.

RESULTS AND DISCUSSION

The as-prepared a-PMMA-C_{60} composites are quite homogeneous as revealed by light, scanning and transmission electron micrographs (Fig. 1 shows TEM micrographs) of the PMMA-C_{60} films. Hence, even at a filler volume concentration of 5% a good dispersion of the filler in a-PMMA matrix was obtained. The dispersion is additionally probed by WAXD data (see below). Fig. 2 shows TDMS spectra (desorption rate, dN_{MMA}/dt, of PMMA monomer—MMA versus temperature) for neat a-PMMA, a-PMMA-MWNT, and a-PMMA-C_{60} composites prepared by SD technique. MMA monomer desorption was registered for several peaks of MMA mass-spectrum (m/z = 41, 69, 39, 100) of this molecule tabulated for the experimental conditions used in our measurements. The comparison of the TD spectra of neat a-PMMA and a-PMMA filled with MWNT evidences that they are almost indiscernible. It is pertinent to note here that according to TEM images of our PMMA-MWNT composites the dispersion of nanotubes is good. Dispersion ranges from well dispersed single nanotubes to the regions of dense nanotube networks. Example of the structures observed in PMMA-MWNT composites is given

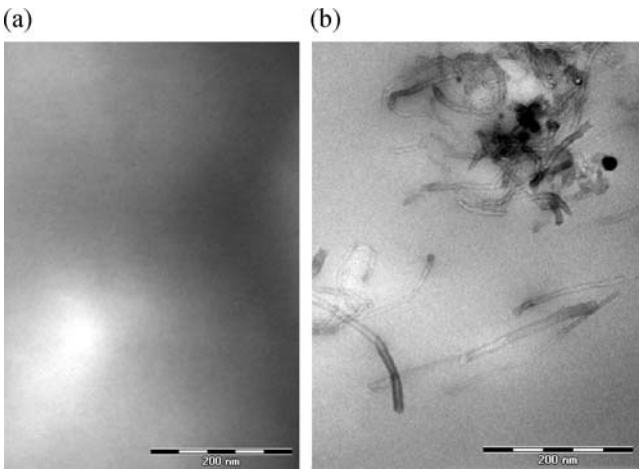

Figure 1. Typical TEM micrographs of the PMMA-C_{60} composites (a) and PMMA-MWNT (b) composites.

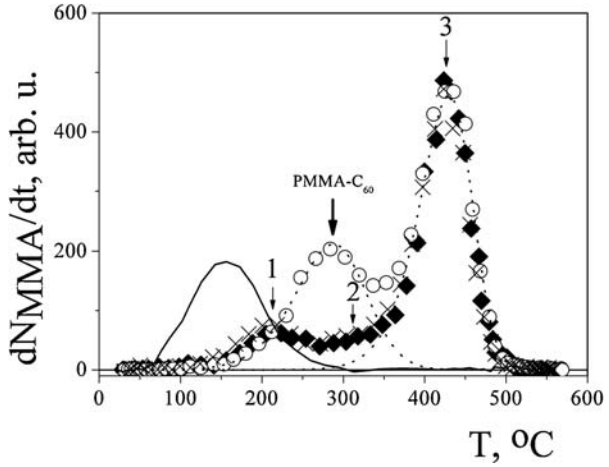

Figure 2. TD spectra (dependency of the rate of the MMA monomer desorption on sample temperature) for neat PMMA (solid diamonds), PMMA-MWNT composite (crosses) and PMMA-C_{60} (empty circles) composites. The curve shown as a solid line presents the toluene TD spectrum. Three thin vertical arrows denoted as 1, 2, and 3 show the temperatures of the maxima of the elementary TD stages of neat PMMA usually ascribed to, respectively, head-to-head weak bonds dissociation, dissociation of end groups, and dissociation of macromolecule at random sites (see text). The thick vertical arrow shows the stage of TD spectrum due to the presence of C_{60} (PMMA-C_{60} feature). The spectra are normalized by the intensity of the high temperature stage. Dotted curves are the fitting solutions of kinetic equations (see text for explanation). Heating rate $\sim 8\,K\,s^{-1}$ at the maximum of the spectra.

in Fig. 1b. Even though the dispersion of nanotubes is to be further ameliorated, we note that the PMMA-nanotube interface area is fairly high in the composites studied.

The TD spectra of SD films of a-PMMA-C_{60} composite, however, contain most easily discerned additional TD stage indicated by a thick vertical arrow in Fig. 2 (PMMA-C_{60} feature). This stage is less pronounced for RD films. This stage means a lower thermal stability of a-PMMA-C_{60} composite compared to neat PMMA. These results agree with the lower thermal stability reported for a-PMMA-C_{60} films (observed by optical microscopy) in Reference [18] compared to syndiotactic, st-, rich PMMA-C_{60} composite. This was attributed to higher crystallinity of st-PMMA-C_{60} inclusion complex. One can expect that this difference can manifest itself in the TD spectra of MMA for st-PMMA-C_{60} composite. TDMS does not reveal any significant shift in the high temperature TD stage attributed to degradation at random sites of the macromolecule (thin vertical arrow 3 in Fig. 2) for a-PMMA-C_{60} composite. Formation of additional TD stage for a-PMMA-C_{60} composite and absence of C_{60} influence on the high temperature TD stage are principal in this paper. It is, therefore, an aim of further part of the paper to compare these results with the data of other thermal and spectroscopic approaches. Furthermore the toluene desorption recorded immediately (see Fig. 2) begins at temperatures which are lower than the low temperature stages of MMA monomer TD spectrum. However, the solvent is still present at the temperatures when the low-temperature MMA desorption stages take place. Therefore in considering the changes in these stages one has to account on the presence of the solvent in the film.

TD spectra were fitted by solutions of kinetic equations. First note, that the TD spectrum of neat a-PMMA (see Fig. 2) contains at least three elementary stages (shown as vertical arrows 1, 2, 3) usually related to decomposition initiated at weak head-to-head, end groups of the macromolecule (arrows 1, 2, respectively) and (arrow 3) at random sites of macromolecule.[10] This is in agreement with the atacticity of the PMMA used in this study. The fit of TD spectrum of PMMA-C_{60} composite is restricted by two calculated curves in Fig. 2. We also note that the fitting results in effective activation energies of ~150 kJ/mol and ~50 kJ/mol for high temperature TD stage and for low temperature "PMMA-C_{60}" stage, respectively. Detailed fitting of the TD spectra of MMA may need more complicated kinetic schemes (see e.g. Reference [19] and references therein for details) and requires further computational efforts. However, the activation energies we present are quite reasonable and are indicative of the weakening of PMMA bonds induced by C_{60}—a molecule with good electron acceptor properties (electron affinity of C_{60} is 2.689 eV).[20]

A significant broadening of ^{1}H NMR lines for PMMA-MWNT composites dissolved in deuterated chloroform compared to those of neat PMMA and PMMA-C_{60} composites (see Fig. 3a) is observed. The cross sign (x) in the NMR spectrum (Fig. 3a) indicates the line attributed to residual toluene in chloroform solutions of the composites. The spectra of PMMA and PMMA-C_{60} composites are almost indistinguishable. The observed broadening of the NMR lines of PMMA-MWNT composite is tentatively attributed to the effects of certain spin relaxations.[21] Though more thorough study of this effect is under way it is important to note that it does not result in measurable difference in the pattern of the composite degradation compared to neat PMMA neither revealed by TDMS approach nor by TGA (see below).

In addition to NMR measurements, EPR data on the initial stages of a-PMMA-C_{60} composite degradation were obtained. EPR spectra of a-PMMA/C_{60} samples before and after annealing (at ~170°C during 2 hr in vacuum of ~100 mbar) are shown in Fig. 3b. In the a-PMMA-C_{60} sample before heating one observes only single EPR line (curve 1 in Fig. 3b) with $g = 2.0020$ and $\Delta H_{pp} = 1.6$ G. This line originates from C_{60}-oxygen complex.[22–26] Upon thermal treatment of the composite two additional EPR lines, b and c (Fig. 3b, curve 2), with the parameters $g = 2.0026$; $\Delta H_{pp} = 9.6$ G and $g = 2.0$; $\Delta H_{pp} = 2.2$ G, respectively, appear.

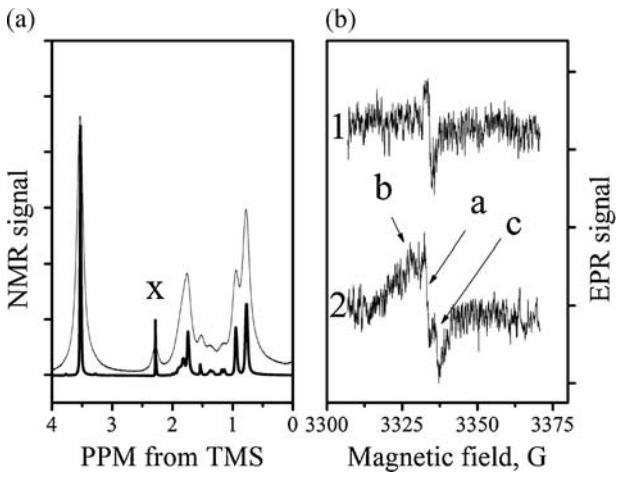

Figure 3. (a) ^{1}H NMR spectra of PMMA-C_{60} (thick line) and PMMA-MWNT (thin line) composites dissolved in deuterated chloroform. Cross sign X denotes NMR signal of residual toluene. (b) EPR spectra taken at room temperature for PMMA-C_{60} composite before (curve 1) and after (curve 2) heat treatment at ~170°C in dynamic vacuum of ~4 mbar.

These parameters slightly change as a function of thermal decomposition processes, but *g*-value of line b remains always higher than free electron *g*-value ($g = 2.0023$), and *g*-value of line c remains less than 2.0023. Taking into account the results of numerous studies of photo- and thermally stimulated reactions in polymer/C_{60} composites[27–31] we can confidently conclude that EPR lines b and c originate from paramagnetic defects in the macromolecules (probably of polaron nature) and fullerene anion radical C_{60}^- radical (adducts C_{60}/polymeric chain), respectively. Note that these interaction mechanisms are in a good agreement with those found in Reference [32] for polyvinylpyrrolidone-C_{60} composite and explained by electron charge transfer between carbonyl group and C_{60}. The presence of carbonyl group in PMMA suggests the similarity of the interaction mechanisms in these composite systems. Currently we elaborate molecular level mechanisms of thermally induced changes involving the formation of anion C_{60}^- radical and the polaron defect, P^+, on PMMA macromolecule ($PMMA + C_{60} \rightarrow P^+ + C_{60}^-$) at low temperature depolymerization (see PMMA-C_{60} stage in Fig. 2) of "PMMA-C_{60}" composite.[33]

Now consider the data on weight loss kinetics as measured by TGA. Figure 4 shows DTGA curves (time differential of the time dependence of the sample mass, -dm(t)/dt, versus temperature) of neat a-PMMA, a-PMMA-MWNT, and a-PMMA-C_{60} composites prepared by SD and RD techniques. The mass loss of the samples proceeds through two stages in the temperature ranges of 100–300°C and 300–450°C. The first stage corresponds to the evaporation of solvent. This is supported by TD spectrum of toluene (see Fig. 2) taken from the samples. This stage almost coincides with the high temperature stage of DSC curves obtained upon first scan of the samples (see additional curves in upper part of Fig. 4). The high temperature stage of DTGA curves is attributed to degradation at random sites of the macromolecules and corresponds to that marked as thin vertical arrow 3 in Fig. 2. First note that the DTGA curve for a-PMMA-MWNT composite is almost indiscernible from that of neat a-PMMA. On the other hand, DTGA high temperature peak strongly shifts to higher temperatures for a-PMMA-C_{60} composites compared to neat a-PMMA. This shift is more pronounced for RD a-PMMA-C_{60} composite samples. It is clear that this observation is in a contradiction with the TDMS data on these samples presented in Fig. 2. Our tentative explanation of this contradiction was discussed in Reference [12], where it was shown that contrary to TGA technique the TDMS approach implies smaller concentration gradients and diffusion relaxation times (L^2/D, where L—linear size of the sample, D—diffusion coefficient of penetrant molecule) because of smaller sample size used in TDMS experiments (compare L $\sim$1 μm for TDMS and $\sim$1000 μm for TGA experiments which means about 10^6 times difference in respective diffusion relaxation times). For typical D value of the monomer in the polymer melt of $\sim 10^{-10}$ m^2/sec[34] we obtain the diffusion relaxation times of $\sim 10^{-2}$ sec for TDMS (this value is well below the temporal step of TD spectrum registration) and 10^4 sec for TGA experiments, respectively. Consequently, a more precise real thermal decomposition kinetics is expected in TDMS experiments. However, the observed shift in DTGA curves can be tentatively explained by the changes in certain physical properties of the composite (e.g. thermal diffusivity of the sample material and/or its diffusivity toward the penetrant molecules, e.g. MMA). Note that the thermal diffusivity was shown to change for PMMA-C_{60} composites compared to neat PMMA.[35] With this regard, the role of dispersion as a factor which influences the mass loss of the composite sample can become quite important due to strong dependence of specific surface area on particle size. For example, the specific surface area for a sphere with the diameter d is proportional to 6/d. The shift of the DTGA peaks to higher temperatures observed for composite films should be additionally understood in terms of these factors. Note also that in recent work,[36] the authors used rapid precipitation method (similar to RD method of samples preparation discussed in our paper) of composite formation and obtained a good dispersion of C_{60} fullerenes in polystyrene matrix with a volume concentration of about 5%. The solvent evaporation method resulted in a poorer degree of dispersion compared to the rapid precipitation method and a lower thermal stability revealed by TGA at constant temperature. There are hopes to obtain higher values of C_{60} in molecularly dispersed state for PMMA matrix.

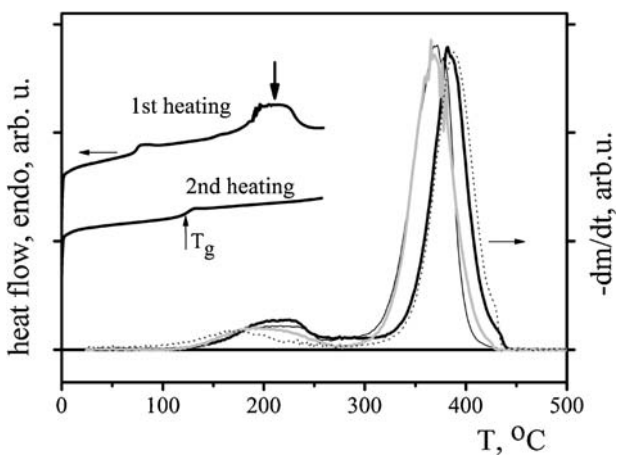

Figure 4. DTGA (dependence of rate of mass loss, dm/dt, on temperature) curves of neat a-PMMA (thin solid line), a-PMMA-MWNT composite (solid grey line), a-PMMA-C_{60} composite prepared in SD conditions (thick solid line) and a-PMMA-C_{60} composite prepared in RD conditions (thin dotted line). See text for details. Upper curves show DSC data for a-PMMA-C_{60} SD composite upon first and second heating runs of the same sample. Heating rate of 10 K min^{-1} was used in all experiments.

It is natural to expect that different drying conditions may lead to different dispersion of C_{60} molecules in a-PMMA matrix. Our TEM images do not reveal fullerene-containing particles in PMMA-C_{60} composites (Fig. 1a). In addition, as is seen from WAXD data (Fig. 5) the PMMA-C_{60} composites do not contain reflections of neat C_{60}, that is fullerene is X-ray amorphous in our composite samples prior to heating. Certain order of the composite, however, manifests itself by the presence of halos in WAXD diagrams. Experiments show that the halo intensity is strongly dependent on the preparation conditions of the composite, presence of solvent and fullerene molecules. For example, it is clear from WAXD diagram that PMMA-C_{60} RD composite exhibits a much less intense halo at $\sim$18°. The positions of the halos may be attributed to certain ordered structures, e.g. stereocomplexes,[37] PMMA-C_{60} peapods,[7] etc. The melting of the stereocomplexes was indeed reported in several papers as an endothermic process by DSC at $\sim$200°C see, e.g. Reference [38]. In our study this endotherm is observed on first heating but disappears after solvent removal (see thick vertical arrow in Fig. 4). The halo intensity redistribution in PMMA-C_{60} composites is, alternatively, ascribed to the nuclei of C_{60} crystallites.[11] Further studies are obviously needed to elucidate the specific influence of these separate factors on the supermolecular

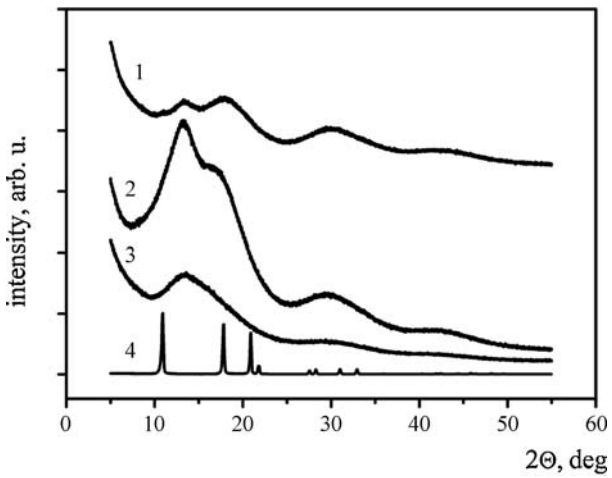

Figure 5. WAXD spectra of neat a-PMMA (1), a-PMMA-C_{60} SD composite (2), a-PMMA-C_{60} RD composite (3) and fullerene C_{60} powder (4) used in the work. According to TGA data the volume content of toluene in the polymer samples is ~8%.

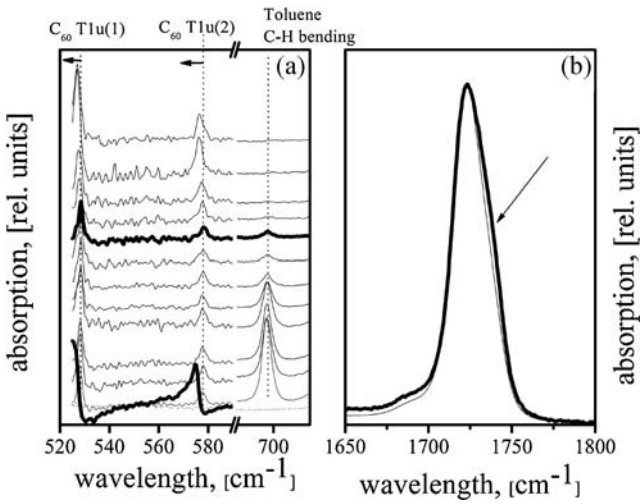

Figure 6. (a) FT-IR spectra of PMMA-C_{60} composite after dynamic vacuum (~4 mbar) treatment at different temperatures (from bottom to the top: room temperature, 50, 110, 115, 123, 140, 150, 160, 170 (thick line marks the crossover to almost toluene-free material as well as the onset of visible shift of C_{60} lines), 180, 200, 220, and 240°C. The spectrum of neat PMMA block is shown as a dotted curve at the bottom of the graph. The spectrum of neat C_{60} is also shown as thick solid curve at the bottom of the graph. The onset of the signal registration in the apparatus available in this study determines the onset of the curves along abscissa axis. (b) another FT-IR spectrum region of PMMA (thin line) and PMMA-C_{60} composite (thick line) at room temperature (see text).

structures as well as on the thermal stability of the composites. Therefore, in thermal decomposition experiments (e.g. TDMS and TGA) one has to control these structural characteristics more carefully in order to compare the thermal stability of the composites accounting, additionally, on PMMA stereoregularity and molecular weight.

Pure fullerenes C_{60} have upon heating a simple cubic to face-centered cubic crystal structure transition at around −15°C.[39] This is indeed observed in our DSC experiments on neat fullerene (not presented). However, this transition is not detected for a-PMMA-C_{60} composites. Therefore, DSC supports the WAXD suggestion of good dispersion of C_{60} in the a-PMMA matrix for our composite samples.

FT-IR data for the composite samples annealed at different temperatures are shown in Fig. 6. The two peaks seen in Fig. 6a at approximately 527 and 577 cm^{-1} correspond to $T_{1u}(1)$ and $T_{1u}(2)$ fundamental vibrational modes of C_{60} molecule. The horizontal arrows in the figure show the direction of the shift of the position of the lines upon heating the sample (the curve obtained for the sample shown with bold solid line corresponds to the heat treatment temperature of 180°C—the temperature of the onset of measurable shift in position of the lines). This temperature corresponds well with EPR data probably implying, though not unequivocally, the similar molecular mechanism underlying these changes. Note that prior to heating the position of the lines is shifted to higher wavenumbers compared to the lines of neat fullerene C_{60} (thick curve at the bottom of the Fig. 6a) indicating the higher frequency of vibrations of fullerene molecules in the composites. The heating of the samples above ~180°C results in the shift of these lines to lower wavenumbers (toward those of neat fullerene). Since the position of vibrational modes can be sensitive to the changes in the icosahedral symmetry of the C_{60}, e.g. due to certain interactions between fullerene and matrix already at low temperatures, this may mean that the interactions of PMMA and C_{60} are realized already at low temperatures. FT-IR data suggest, therefore, that the increase in temperature probably leads to a loss of certain interactions between the matrix and the fullerene molecules. It is also important to note that the onset of this shift starts at temperatures when the infra-red lines of toluene (see Fig. 6a) almost disappear and corresponds well to the low temperature depolymerization of PMMA-C_{60} composite (see TD stage of PMMA-C_{60} composite in Figure 2). The latter can indicate that the a-PMMA-C_{60} interactions are probably supported by the presence of toluene molecules in the matrix as well as by the presence of specific conformations of macromolecules supporting these interactions. Note here that observation of FT-IR spectra in the wavelength range corresponding to the vibrations of carbonyl band (Fig. 6b) does not enable us to reveal reliable difference between PMMA and its composite which may signal on the differences in aggregation of PMMA[40] induced by C_{60}. We note only somewhat asymmetric shape of the curves and slight increase of high wavelength shoulder for PMMA-C_{60} composite shown with an arrow in Fig. 6b.

CONCLUSIONS

We have compared TDMS spectra of thin films of neat a-PMMA and its composites with C_{60} fullerene and MWNT. The data evidence that fullerene C_{60} present in PMMA matrix induces low temperature formation of PMMA monomer compared to neat PMMA. According to TDMS analysis the high temperature stage of a-PMMA degradation at random sites is unaffected by the presence of C_{60}. Contrary to TDMS data, TGA analysis shows that the high temperature stage of a-PMMA degradation in a-PMMA-C_{60} samples is shifted to higher temperatures compared to neat a-PMMA. The contradiction between TDMS and TGA data is tentatively explained by the difference in the experimental conditions of the experiments, in particular, by the comparatively large size of the samples used in TGA experiments. Reduction of thermal stability is supported by EPR technique. EPR spectra

suggest increased rate of thermally induced defects formation in the a-PMMA-C_{60} composites compared to neat a-PMMA and a-PMMA-MWNT composite.

Acknowledgements

Aleksei O. Pozdnyakov thanks the Collaborative Research Centre SFB 481 of the University of Bayreuth for the support of the studies at the University of Bayreuth and Russian Foundation for Basic Research grants No. 09-08-90410-UKR_f_a, 10-08-90000-Bel_a and 09-08-01076-a for the support of TDMS studies. Andrei A. Konchits thanks Ukraine Scientific Foundation of Fundamental Research grant No. F28/418-2009 for support of EPR studies. The authors also gratefully acknowledge the experimental support and discussions with Dr Dominik Erhard (nuclear magnetic resonance), Dr Wolfgang Milius (wide-angle diffraction measurements), Mr Andreas Haedler (nuclear magnetic resonance), Mrs Ute Kuhn (differential scanning calorimetry), Mrs Carmen Kunert (electron microscopy), Mrs Anne Lang (electron microscopy), and Mrs Christina Löffler (gel permeation chromatography).

REFERENCES

[1] P. M. Ajayan, L. S. Schadler, P. V. Braun, *Nanocomposite Science and Technology*, Wiley-VCH, Verlag, Weinheim, **2003**.
[2] *Progress in Fullerene Research* (Ed: L. Milton), Nova Science Publishers, New York, **2007**.
[3] *Fullerene Research Advances* (Ed: C. N. Kramer), Nova Science Publishers, New York, **2007**.
[4] K. M. Kadish, R. S. Ruoff, *Fullerenes: Chemistry, Physics, and Technology*, Wiley-Interscience, New York, **2000**.
[5] J. M. Kropka, K. W. Putz, V. Pryamitsyn, V. Ganesan, P. F. Green, *Macromolecules* **2007**, *40*(15), 5424.
[6] J. M. Guenet, *Thermoreversible Gelation of Polymers and Biopolymers*, Academic Press Ltd., London, **1992**.
[7] T. Kawauchi, J. Kumaki, A. Kitaura, K. Okoshi, H. Kusanagi, K. Kobayashi, T. Sugai, H. Shinohara, E. Yashima, *Angew. Chem.* **2008**, *120*, 525.
[8] M. E. Mackay, A. Tuteja, P. h. M. Duxbury, C. J. Hawker, B. V. Horn, Y. Guan, G. Chen, R. S. Krishnan, *Science* **2006**, *311*, 1740.
[9] P. J. Flory, *Principles of Polymer Chemistry*, Cornell University Press, Ithaca, New York, **1953**.
[10] T. Kashiwagi, A. Inaba, J. E. Brown, K. Hatada, T. Kitayama, E. Masuda, *Macromolecules* **1986**, *19*, 2160.
[11] B. M. Ginzburg, A. S. Smirnov, S. K. Filatov, L. A. Shibaev, E. Y. Melenevskaya, A. V. Novoselova, A. A. Shepelevskii, *Tech. Phys. Lett.* **2003**, *76*(3), 457.
[12] A. O. Pozdnyakov, *Fullerene Research Advances*, Chapter 4, (Ed: C. N. Kramer), Nova Science Publishers, New York, **2007**, 97–115.
[13] L. A. Shibaev, T. A. Antonova, L. V. Vinogradova, B. M. Ginzburg, V. N. Zgonnik, E. Y. Melenevskaja, *Tech. Phys. Lett.* **1997**, *23*, 81.
[14] B. B. Troitskii, L. S. Troitskaja, A. S. Yakhnov, M. A. Lopatin, M. A. Novikova, *Eur. Polym. J.* **1997**, *33*, 1587.
[15] B. B. Troitskii, L. S. Troitskaja, A. S. Yakhnov, A. A. Dmitriev, V. N. Denisova, M. A. Novikova, L. I. Anikina, G. A. Domrachev, *Dokl. Akad. Nauk.* **1998**, *363*, 79.
[16] B. B. Troitskii, L. S. Troitskaja, A. A. Dmitriev, A. S. Yakhnov, *Eur. Polym. J.* **2000**, *36*, 1073.
[17] B. B. Troitskii, G. A. Domrachev, L. V. Khokhlova, L. I. Anikina, *Vysokomol. Soedin.* **2001**, *A43*, 1540.
[18] M. Kawauchi, T. Kawauchi, T. Takeichi, *Macromolecules* **2009**, *42*, 6136.
[19] B. J. McCoy, *Ind. Eng. Chem. Res.* **1999**, *38*, 4531.
[20] X-B. Wang, Ch. -F. Ding, L-Sh. Wang, *J. Chem. Phys.* **1999**, *110*(17), 8217.
[21] F. A. Bovey, G. V. D. Tiers, G. Filipovich, *J. Polym. Sci. 38*, **1959**, 73.
[22] M. D. Pace, T. C. Christidis, J. J. Yin, J. Milliken, *J. Phys. Chem.* **1992**, *96*(17), 6855.
[23] Y. Maniwa, M. Nagasaka, A. Ohi, K. Kume, K. Kikuchi, K. Saito, I. Ikemoto, S. h. Suzuki, Y. Achiba, *Jpn. J. Appl. Phys.* **1994**, *33*, L173.
[24] P. Paul, R. D. Bolskar, A. M. Clark, C. h. A. Reed, *Chem. Commun.* **2000**, 1229.
[25] P. Paul, K-Ch. Kim, D. Sun, P. D. W. Boyd, Ch. A. Reed, *J. Am. Chem. Soc.* **2002**, *124*(16), 4394.
[26] M. Yu, A. V. Shul'ga, V. M. Kulikov, V. V. Martynenko, V. G. Open'ko, Y. u. Karatevskii, G. Morozov, *Russ. J. Phys. Chem. A* **2008**, *82*(8), 1314.
[27] M. D. Pace, *Appl. Magn. Reson.* **1996**, *11*, 253.
[28] G. Zoriniants, V. Dyakonov, M. Scharber, C. J. Brabec, R. A. J. Janssen, J. C. Hummelend, N. S. Sariciftci, *Synth. Metals* **1999**, *102*, (1-3) 1241.
[29] S. h. Fukuzumi, H. Mori, T. Suenobu, H. Imahori, X. Gao, K. M. Kadish, *J. Phys. Chem. A* **2000**, *104*(46), 10688.
[30] K. Marumoto, M. Kato, H. Kondo, S. Kuroda, N. C. Greenham, R. H. Friend, Y. Shimoi, S. Abe, *Phys. Rev. B* **2009**, *79*, 245204.
[31] V. I. Krinichnyi, E. I. Yudanova, *J. Renew. Sustain. Energy* **2009**, *1*, 043110.
[32] Y. H. Chen, I. I. Khairullin, M. P. Suen, L. P. Hwang, *Fullerene Sci. Technol.* **1999**, *7*(5), 807.
[33] A. O. Pozdnyakov, U. A. Handge, A. A. Konchits, V. Altstädt, *Tech. Phys. Lett. 36*(20), **2010**, 67.
[34] J. L. Duda, G. K. Kimmerly, W. L. Sigelko, J. S. Vrentas, *Ind. Eng. Chem. Fundam. 12*(1), **1973**, 133–136.
[35] T. Kh. Salihov, S. Kh. Tabarov, D. Rashidov, Sh. Tuichiev, A. Hussain, *Tech. Phys. Lett.* **2009**, *35*(11), 1010.
[36] A. Tuteja, Ph. M. Duxbury, M. E. Mackay, *Macromolecules* **2007**, *40*, 9427.
[37] R. Lovell, A. H. Windle, *Macromolecules* **1981**, *14*, 211.
[38] J. Wang, J. Zhao, Q. Gu, D. Shen, *Macromol. Rapid Commun.* **2001**, *22*(12), 948.
[39] P. A. Heiney, J. E. Fisher, A. R. McGhie, W. J. Romanow, A. M. Denenstein, J. P. McCauley, Jr., A. B. Smith, *Phys. Rev. Lett.* **1991**, *66*(22), 2911.
[40] J. Spevacek, B. Schneider, J. Dybal, J. Strokr, J. Baldrian, *J. Polym. Sci., Polym. Phys. Ed. V. 22*, **1984**, 617.

